Transportation Research Part D 117 (2023) 103667

Contents lists available at ScienceDirect

Transportation Research Part D

journal homepage: www.elsevier.com/locate/trd

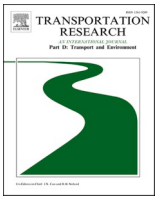

Emissions from railways: Results of tests on a pantograph-catenary test bench

Daniel Fruhwirt [a,*], Peter Sturm [a], Giuseppe Bucca [b], Gina Bode [c], Sabrina Michael [c], Johannes Rodler [d]

[a] Graz University of Technology, Austria
[b] Politecnico di Milano, Italy
[c] German Centre for Rail Traffic Research at the Federal Railway Authority, Germany
[d] FVTmbH, Austria

A B S T R A C T

Many railway tracks have been electrified, thus eliminating exhaust emissions. However, railways still emit particles due to abrasion and wear. The main such particle sources are brakes, wheel-rail contact, and pantographs and contact wire. However, information on the quantities of such particles is rare. Estimations in published data are quite heterogeneous, with PM10 emission levels varying by a factor of ten. In an attempt to improve the database and to reduce uncertainties, a series of test bench tests was conducted on pantograph-catenary contact. In order to study the impact of specific parameters, i.e. of train speed, contact force and current intensity, on the emitted particle mass and size distribution, parameter levels were varied across the tests. A chemical analysis of emitted particles provided information on the respective contributions of contact strip and contact wire. PM10 emission factors were found to lie in the range of 0.14–0.62 g/km.

1. Introduction

Exhaust emissions in rail transport are gradually being eliminated as more and more railway lines become electrified. This applies specifically to the European Union where on average 57% of the railway tracks are electrified. Nevertheless, this number varies greatly between the individual member states. While 61% of German railway tracks are electrified the highest electrification rates within the European Union can be found in Luxembourg (91%) and Belgium (88%) (Allianz pro Schiene e.V., 2022). Railways have been a key factor in Switzerland's transport strategy for several decades. The result is an impressive 100% electrification rate. However, due to abrasion and wear effects railways still emit a significant number of particles. This includes particles of fractions PM10, PM2.5 and PM1, as well as ultrafine particles in the range of 5–100 nm. (Heldestab, 2002) put the share of rail transport in total PM10 emissions in Switzerland at 11% (2800 to/a). This underlines the importance of railway emissions in air quality. Growing awareness of this issue has led some researchers to investigate the non-exhaust particle emissions from railways (e.g., Abbasi et al., 2013, 2011; Abbasi et al., 2012a, 2012b; Olofsson et al., 2013). Different methods were used for this purpose. The most simple approach is an analytical one, taking the material loss and replacement cycles of railway components as an indicator (Burkhardt et al., 2008; Heldestab, 2002; Heldestab and Kljun, 2007). However, this simple mass balance does not provide any information about the size of the particles, their distribution in the environment, and their relevance to health. Alternative methods are found in experimental studies that include field measurements (Fridell et al., 2010), (Sturm et al., 2022), on-board measurements (Cha et al., 2018), and measurements on test benches

* Corresponding author at: Institute of Thermodynamics and Sustainable Propulsion Systems, Graz University of Technology, Inffeldgasse 25c, 8010 Graz, Austria
E-mail address: fruhwirt@ivt.tugraz.at (D. Fruhwirt).

https://doi.org/10.1016/j.trd.2023.103667
Received 8 January 2023; Received in revised form 16 February 2023; Accepted 16 February 2023
Available online 24 February 2023

(Anders Söderberg et al., 2008). While the analytical approach provides an averaged emission factor, experimental studies cover different driving situations. The different boundary conditions and methodical approaches employed in the tests led to a wide range of emission factors for railways. As shown in Table 1 the emission factors vary by a factor of ten.

The consequences for humans have been investigated by (Mohsen et al., 2018) who highlighted the emitted particles with respect to their impact on respiratory problems, cardiovascular problems and carcinogenic effects. In this context, the chemical composition of particles is of great importance. Obviously, in railway transport the heavy metal content is assumed to be high. Chemical analysis of the emitted particles shows that iron (Fe), silicon (Si), magnesium (Mg), copper (Cu), manganese (Mn), silver (Ag) and carbon (TC) are the most prominent elements within the emissions from railways (Fridell et al., 2011; Abbasi et al., 2012a, 2012b; Fruhwirt et al., 2021). Materials from pantograph and contact wire were also identified in these studies. Basically, four different types of contact wires are in use on European railway tracks (Siemens Mobility Global, 2021).

- Pure copper (Cu-ETP)
- Copper – Tin (Cu-Sn)
- Copper – Silver (Cu-Ag)
- Copper – Magnesium (Cu-Mg)

Which type of contact wire is used depends strongly on the electrical and mechanical requirements of the train operators. Current collector strips are often made of steel, copper alloy, pure carbon and metal impregnated carbon. All these have different abrasion properties in interaction with the contact wire (Jiqin, 2018).

In recent years, there has been an increasing interest in the dispersion of abrasion emissions in the environment, especially in water bodies and soil. Therefore, various studies investigated the exposure of heavy metals from railways into the environment. (Samarska et al., 2020) reported the contamination of track ballast by heavy metals in the concentration sequence of Fe > Mn > Cu > Cr > Ni > Zn > Pb > As. Similar results were found by (Zingelmann et al., 2022), in Germany, where an increased heavy metal concentration, i.e. copper and iron, was measured in soil and seepage water samples along railway tracks. A decrease in concentration was found with increasing distance to the tracks. As main source for copper emission, the abrasion from contact-wires was identified and emissions of 6480 g/wire-km were determined (Burkhardt et al., 2008).

Anthropogenic heavy metal emissions are mostly bound at humic matter or organomineral surfaces in soil. The mobility of heavy metals in soil is influenced by different soil properties, in particular the pH value (Landesamt für Bergbau, Energie und Geologie, 2021). A low pH value promotes the mobility, and thus the discharge into the groundwater, of heavy metals. (Landesamt für Bergbau, Energie und Geologie, 2012). Copper accumulates in the environment and eventually reaches hazardous concentrations, which can be toxic for microorganisms (Knauer et al., 1997; Landesamt für Bergbau, Energie und Geologie, 2021; Nirel and Pasquini, 2021).

Several researchers have studied the wear behaviour of both contact strips and contact wires. In (Bucca and Collina, 2015) three different wear mechanisms of contact wire and contact strip were identified: a mechanical contribution due to friction, an electrical contribution due to the Joule effect, and a contribution due to the electrical arc generation which causes particles to be torn out of the material matrix. In order to predict the total wear rate (Bucca and Collina, 2015) developed an analytical model. The aim of this model is to predict the total service life of contact strips and contact wires. Hence, using the model to translate from wear rate to particle emissions is only possible to a limited extent. (Irsigler, 2014) conducted several experiments in order to determine the influence of contact force and current intensity on the wear rate for different types of contact wires. According to Irsigler, a contact wire of pure copper is subject to the highest wear rate, while copper-silver and copper-magnesium contact wires are characterized by a higher mechanical strength. The share of the driving wire pantograph contact in the total abrasion emissions was estimated at approx. 1% (Heldestab, 2002).

Owing to the many uncertainties regarding the total non-exhaust PM emissions from railways and the limited information available in the literature, the current research project (DZSF, 2022) quantifies the abrasion emissions from railroads and the relevance for humans and the environment. This article gives an overview of the first experimental work on contact between pantograph and overhead contact line.

2. Measurement systems and setup

Several tests were carried out in July 2022 on the current collection test bench (CCTB) at Politecnico di Milano (PoliMi). This test bench is able to reproduce the electromechanical contact between a pantograph strip and contact wire, and is as close to real world conditions as possible. One key aspect here is the possibility of generating the relative movement of contact wire and contact strip. In order to generate this movement, the CCTB makes use of a rotating disk (4 m diameter), at which the contact wire is mounted

Table 1
Non-exhaust PM10 emission factors for railways taken from literature.

Publication	Methodology	PM10 emissions factor [g/km]
(Richter et al., 2012)	Analytical – mass loss	3.10–23.10
(Fridell et al., 2010)	Experimental – tunnel measurements	0.24–2.90
(Sturm et al., 2022)	Experimental – tunnel measurements	0.10–2.05
(Fruhwirt et al., 2021)	Experimental – tunnel measurements	0.12–2.00

elastically. In addition, the contact strip is fixed on a sliding bracket that generates a transversal movement to reproduce stagger (zig-zag motion). A hydraulic system additionally enables a vertical movement of the contact strip in order to allow for control of the contact force. This contact force is monitored by an arrangement of load cells. Furthermore, the CCTB is equipped with a supply air/exhaust air system in order to simulate the cooling effect of the airstream and to catch the emitted particles. The technical specifications of the CCTB allow for a variation of driving speed up to 220 km/h. The power supply is optionally provided via 1000 A (DC), 500 A (AC) at 16 2/3 Hz, or 350 A (AC) at 50 Hz. Depending on the test dynamics the voltage level was only in the range of 5–500 V. However, the decisive factor for wear in the contact wire – current collector contact is the amperage (Bucca and Collina, 2009). For this reason, the test bench allows for a control of amperage only. Fig. 1 shows the a basic view on the test bench, as well as a detailed view of the bracket and contact strip. In addition, Fig. 2 shows a schematic picture of.

The emitted particle mass of fractions PM10, PM2.5 and PM1, and the particle number concentration in the range of 5.6 nm to 35 μm, were continuously monitored during the tests. In addition, filter sampling was applied so as to allow chemical analysis of the particles. Due to the high range of parameters to be recorded (e.g., size range of the particles) different particle analysers were employed. The GRIMM Aerosol Technik EDM180 particle analyser was employed to monitor the particle mass concentration as well as the number concentration in the range of 0.25 to 35 μm. This device uses a light scattering technique to count particles. An internal algorithm ultimately transforms the particle numbers of 32 size fractions into a mass concentration for PM10, PM2.5 and PM1. Due to the fact that light scattering does not account for particle density, the calculated particle mass needs to be corrected. Thus, a gravimetric reference measurement system served for the correction of particle mass concentrations. The applied system was a PartisolPlus 2025i sequential air sampler provided by ThermoFisher. In order to enable direct comparison with the EDM180 measurement, the PartisolPlus was equipped with a PM10 separator. In addition, the filter samples from the PartisolPlus sampler were taken for purposes of chemical analysis of the particle composition. Quartz filters were employed, as they enable the chemical analysis of carbon and copper. An engine exhaust particle sizer (EEPS 3090) provided by TSI GmbH served for monitoring the particle number concentrations in the 5.6 to 560 nm range. The EEPS uses sensitive electrometers in combination with three proprietary data inversion matrices in order to count particles in 32 size channels (16 per order of ten) with a time resolution of 1 s. To determine the mass loss of contact wire and contact strip (total suspended particles - TSP), the volume of the contact wire was scanned before and after the test series. The information on the lost volume was used to determine the lost mass by simple multiplication of the volume by the copper density (8.96 g/cm^3). In contrast, mass removal from the contact strip was determined by weighing after each test.

The different particle analysers use sample flows in a range of 1.2 to 16.67 L/min. However, the air velocity in the return air duct reached values up to 61 m/s depending on the simulated train speed. This represents quite a big challenge, as isokinetic sampling is required in order to achieve high accuracy (Kykal et al., 2017). Thus, a system had to be designed which met proper sampling requirements. This sampling system comprised a sample tube, a flexible, antistatic transition piece, a cross-section extension, some fittings, and a horizontal air duct. An image of this set-up is depicted in Fig. 3. The diameter of the sampling tube was 7 cm in order to achieve isokinetic extraction from the return air duct. The opening of this pipe was oriented against the return airflow direction in order to capture a representative sample flow. The subsequent widening of the cross-section (0.25 m diameter) caused a reduction in the flow velocity down to 4.8–5.2 m/s, thus allowing isokinetic sampling with the particle analyser characterized by the lowest sample flow (GRIMM EDM180 – 1.2 L/min; (8) in Fig. 3). In contrast, hyperkinetic sampling, which is assumed less critical in terms of sampling errors, was achieved for the other particle analysers. The sample inlets of the analysers were arranged within a horizontal duct at intervals of roughly 80 cm.

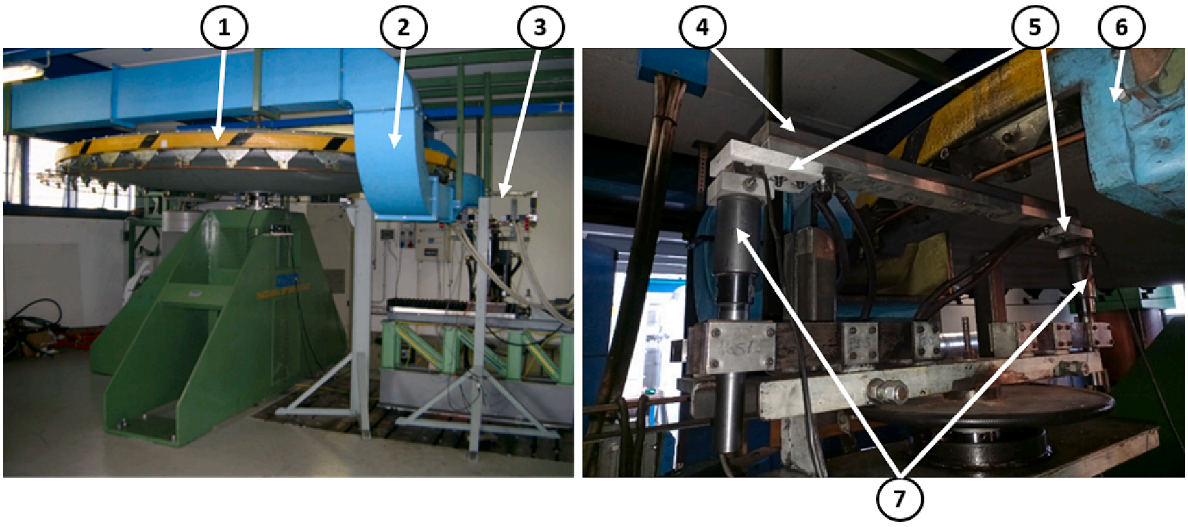

Fig. 1. The current collection test bench (CCTB) at Politecnico di Milano; left: general layout (source: (Politecnico di Milano, 2023)), right – bracket with current collector (1 – rotational disk, 2 – return air duct, 3 – bracket, 4 – contact strip, 5 – load cells, 6 – supply air duct, 7 – hydraulic system).

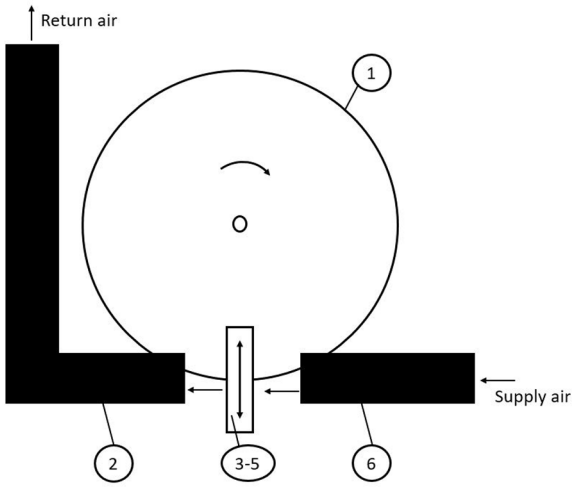

Fig. 2. Scheme of the current collection test bench (CCTB); (1 – rotational disc, 2 – return air duct, 3–5 – bracket with current collector, 6 – supply air duct).

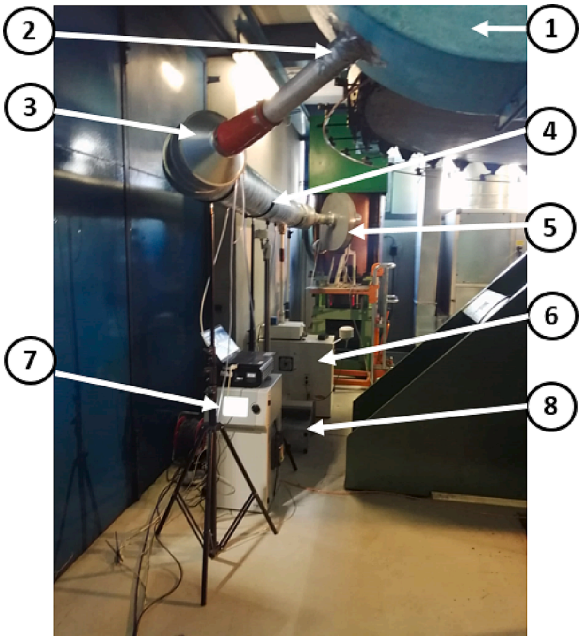

Fig. 3. Sampling route at the PoliMi CCTB including the employed particle analysers. (1 – return air duct, 2 – sampling tube, 3 – cross section expansion, 4 – horizontal duct, 5 – radial fan, 6 – PartisolPlus 2025i (Thermo Fisher Scientific Inc, 2021), 7 – EEPS 3090 (Incorporated, 2022), 8 – EDM180 (Aersol Technik, 2022)).

Table 2
Mechanical and electrical properties of the contact strip.

Bulk density	2.2–2.4 [g/cm^3]
Resistivity	500–700 [μΩ cm]
Flexural strength	90–110 [MPa]
Shore hardness	60–90
Impregnation Cu	20–25 [%]

3. Experimental carrier and test matrix

As already mentioned in section 1, different types of contact wires and contact strips are available on the market and are in use along European railway tracks. Hence, a decision had to be made whether to test the most representative or the worst components in terms of wear behaviour. After some deliberation, the decision was made to use a contact wire of pure copper (Cu-ETP) with a cross-section of 100 mm^2, and an impregnated carbon strip with a width of 60 mm. Both test carriers are widely used in European railway systems. The main specifications of the contact strip are presented in Table 2. Both the contact wire as well as the contact strip were used in the course of the test preparation in order to allow for realistic test conditions. The surface condition of both elements at the beginning of the tests is illustrated in Fig. 4.

Under real driving conditions, the actual emissions from contact between contact wire and contact strip depend on many parameters, e.g., train speed, current intensity, dew or ice formation, etc. The latter could not be simulated in the tests. However, in order to cover a large number of real driving situations, a test matrix comprising 13 tests was defined. These tests were characterized by variations in train speeds, contact forces and current intensity. The train speed was varied in four steps from 60 km/h to a maximum of 220 km/h. A distinction was also made between freight and passenger trains. Three different train speed levels (60 – 80 – 100 km/h) were applied for freight trains and train speeds of 100 km/h, 160 km/h, 200 km/h and 220 km/h were applied in simulating passenger trains. The overlap of train speeds at 100 km/h allowed for a deeper investigation of the impact of contact force, as this parameter was set at 50 N in the freight train test scenarios and at 90 N for passenger train tests. Two different levels of current intensity (500 A and 800 A per strip) were applied on each combination of train speed and contact force. All these variations resulted in the test configurations A to M (see Table 3). The driving distance (50 km) was kept constant for all tests, thus, resulting in a decreasing test duration with increasing train speed.

4. Results

The analysis of particle emissions included observation of particle mass, particle size distribution, and chemical analysis of particle composition. The following sections describe the main findings on these parameters.

4.1. Particle mass

Particle emission from contact between contact wire and contact strip is mainly caused by two different mechanisms. According to (Derosa et al., 2020), these are mechanical friction and electric arcs. In order to determine the influence of these mechanisms and to enable statements to be made concerning the reproducibility of results, most of the tests listed in Table 3 were performed at least twice.

Based on the sum of the mass removal from the contact strip and contact wire, emission factors in [g/km] were obtained by dividing the total mass collected by the driving distance (50 km). The derived emission factors are related to total suspended particles, as the mass loss was determined by weighing the contact strip and laser scanning of the contact wire. In this context, it has to be highlighted that only an average mass loss of all tests could be determined for the contact wire. This is due to the extended scan time that only allowed for a scan before and after the test series. Since the TSP emission factors took into account the average mass loss of the contact wire, a direct comparison with the PM emission factors in Table 4 (weighing of the filter samples after each test) is not possible. Fig. 5 shows these emission factors as a function of train speed. The different colours and symbols indicate the levels of contact force and current intensity, respectively. The TSP emissions for abrasion of contact wire and contact strip ranged from 0.04 to 0.28 g/km. The results differ significantly depending on the test configuration employed. In particular, low contact forces in combination with high train speed favours contact loss and the occurrence of electric arcs. However, the low speed test configuration B (60 km/h|50 N|800 A)

Fig. 4. Condition of the test carriers before the tests.

Table 3
Test matrix covering 12 test scenarios.

Train type	Denotation	Speed [km/h]	Current intensity [A]	Contact force F_s [N]	Driving distance [km]	Test duration [min]
Freight	A	60	500	50	50	50.0
	B		800		50	50.0
	C	80	500	50	50	37.5
	D		800		50	37.5
	E	100	500	50	50	30.0
	F		800		50	30.0
Passenger	G	100	500	90	50	30.0
	H		800		50	30.0
	I	160	500	90	50	18.8
	J		800		50	18.8
	K	200	500	90	50	15.0
	L		800		50	15.0
	M	220	500	90	50	13.6

Table 4
PM10, PM2.5 and PM1 emission factors dependent on the test configuration.

Test	PM10 [g/km]	PM2.5 [g/km]	PM1 [g/km]
A	0.2	0.17	0.14
B	0.45	0.4	0.34
C	0.3	0.26	0.22
D	0.27	0.24	0.21
E	0.27	0.22	0.17
F	0.3	0.26	0.21
G	0.14	0.12	0.10
H	0.31	0.27	0.21
I	0.26	0.22	0.19
J	0.32	0.28	0.24
K	0.57	0.51	0.44
L	0.54	0.48	0.42
M	0.62	0.53	0.46

caused the highest particle emissions. This is probably triggered by the high level of current intensity and low contact force. Hence, electric arcs and a high level of power dissipation due to the Joule effect caused the temperature of the contact strip to increase, and the low train speed did not provide sufficient cooling effect. The increased temperature on the contact strip resulted in poor emission behaviour.

As observed in the tests, mechanical friction is always present. This type of emission behaviour is continuous. In contrast, electric arcs represent single events, normally of short duration, and thus lead to recurring or periodic emissions. The results depicted in Fig. 5 indicate an increase of mechanical friction with increasing train speed and an enhanced contribution of electric arcs for low contact forces and high current intensity.

However, in order to study the impact of train speed, contact force and current intensity in more detail, further analysis was performed. For this deeper analysis, the emission factors of tests with the same test configuration were averaged to enable a better illustration of results. To clarify the specific impact of the parameter under investigation, the others were kept constant. Thus, the analysis had to be done separately for freight trains and passenger trains, as the test configurations were characterized by different contact forces. The result of this analysis can be expressed as shown in Fig. 6, in which the impact of the train speed on the emission factor is depicted. With increasing train speed, quadratic growth in the TSP emission factor was demonstrated for both train types. This confirmed expectations, based on earlier results (Bucca and Collina, 2009), relating to dependency on mechanical friction. According to the test bench, results analysed here, the TSP emission factor for freight trains increases by roughly 33% when the train speed increases from 60 km/h to 100 km/h. In comparison, increasing the speed of passenger trains from 100 km/h to 220 km/h causes TSP emissions to increase by a factor of four. In addition, the offset of the tests at 100 km/h is caused by the deviation of the contact force. Although the effects of arcing had less influence in these tests, the combination of electrical and mechanical influences is still decisive for the emission behaviour. Hence, considering mechanical friction alone will result in a different amount of emitted particles. A similar analysis was performed to determine the impact of contact force and current intensity. The results of these analyses are depicted in Fig. 7 and Fig. 8.

To enable again a single parameter dependency, only emission factors for tests with a train speed of 100 km/h are illustrated in Fig. 7. In addition, the emission factors are depicted separately for low, i.e. 500 A (triangles) and high current intensity, i.e. 800 A (squares). In both cases, the emissions decrease with increasing contact force, as higher contact forces cause less contact losses. Thus, the impact of electric arcs is reduced, although it is still present.

This can be observed by a comparison of the emission factors in test configurations 50 N | 500 A and 90 N| 800 A. As can be seen,

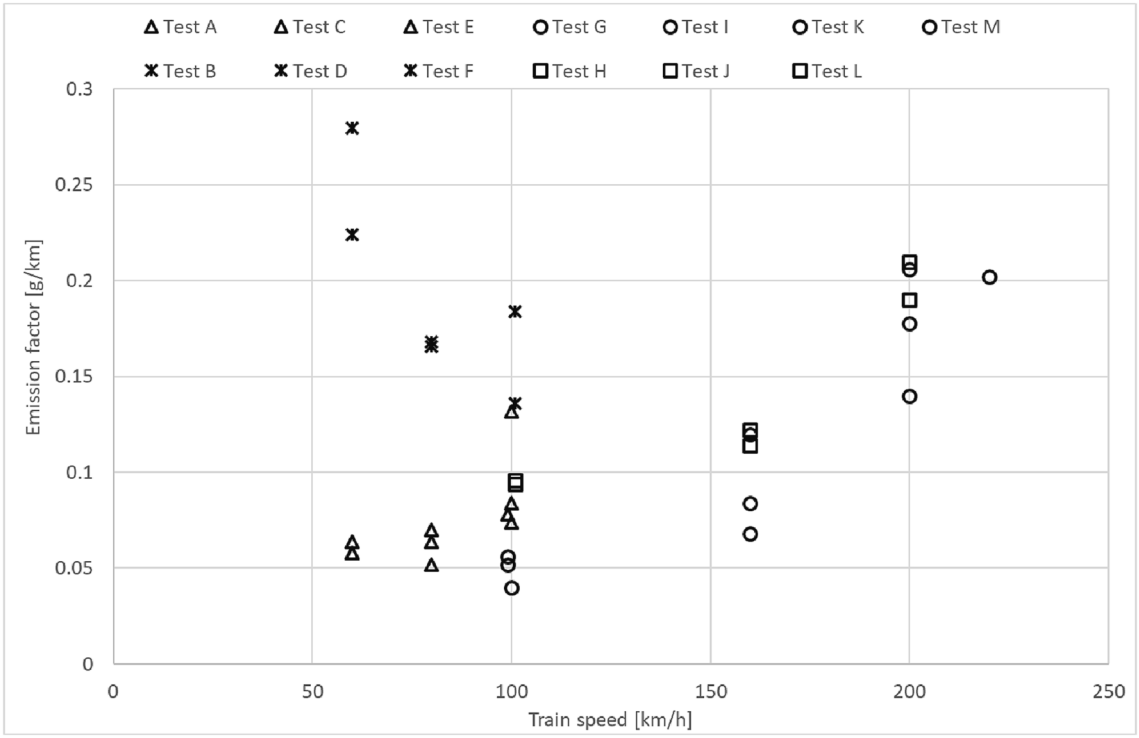

Fig. 5. TSP emission factors plotted against the train speed, as dependent on test configuration (triangles – 50 N|500 A; circles – 90 N|500 A; crosses – 50 N|800 A; squares – 90 N|800 A).

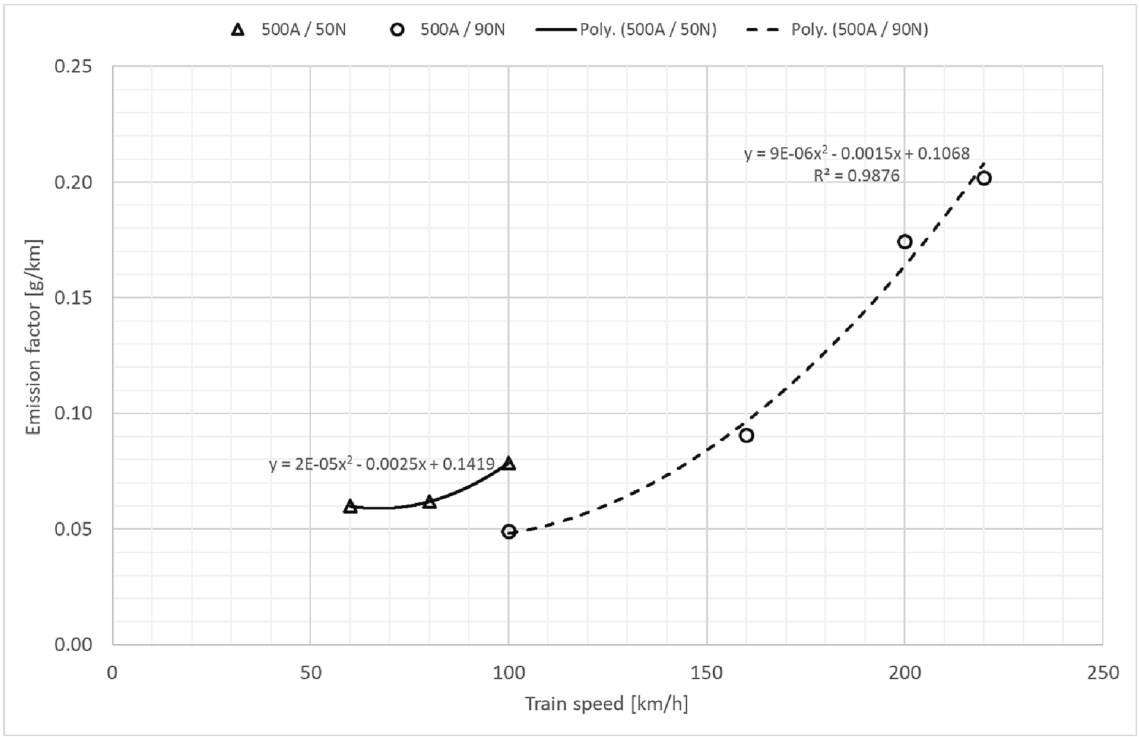

Fig. 6. Impact of train speed on the TSP emission factor.

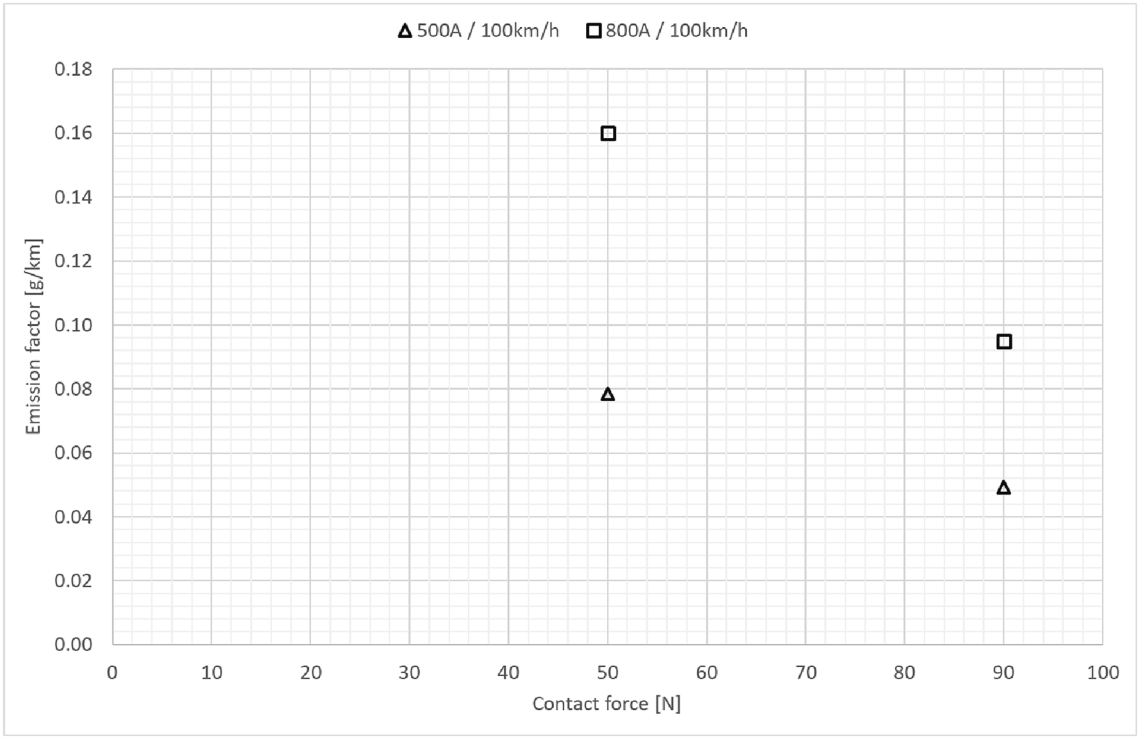

Fig. 7. Impact of contact force on TSP emission factors.

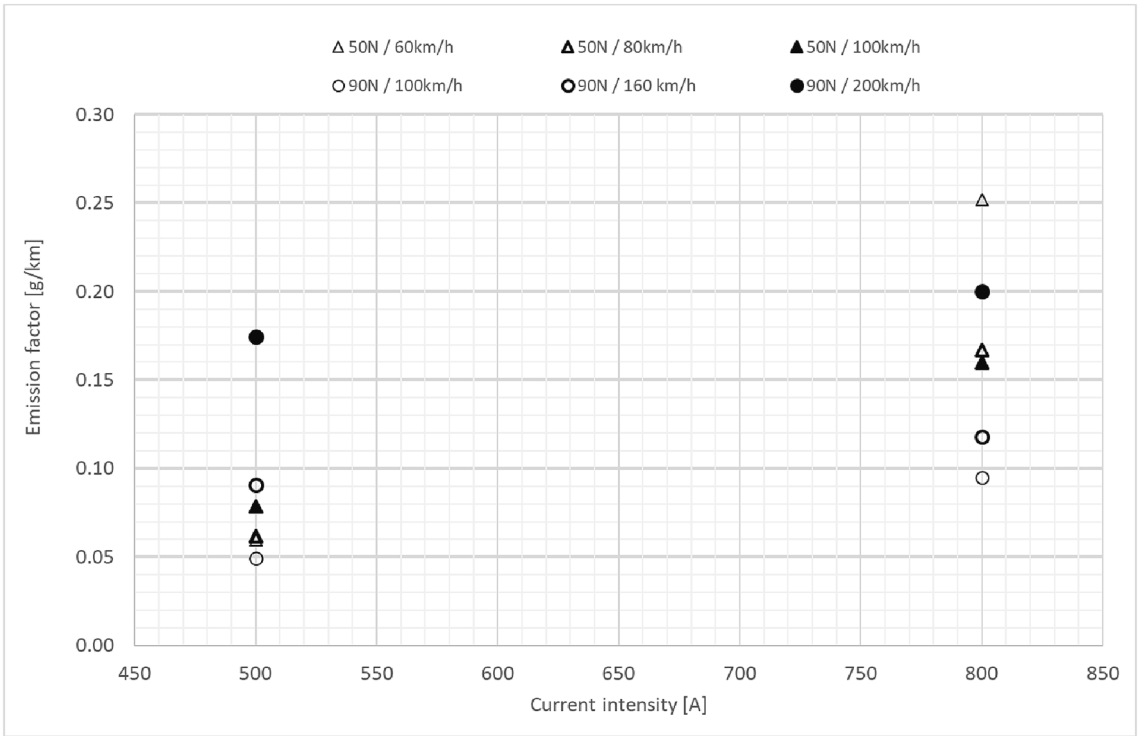

Fig. 8. Impact of current intensity on TSP emission factors.

the latter configuration causes roughly 40% lower emissions than the former. The influence of current intensity on TSP emissions also depends on contact behaviour. The effect of an arc is even stronger at high amperage than at a lower amperage.

This is confirmed by the results shown in Fig. 8. Here, higher amperage always leads to higher emissions, regardless of the train speed and the contact force. However, in the quantification of the increased emissions, the combination of train speed and contact force needs to be taken into account. In this context, the increase of current intensity in scenarios with high contact force (circles in Fig. 8) caused an increase of TSP emissions in the range of 0.025–0.045 g/km. In contrast, in the low contact force scenarios (triangles in Fig. 8) this increase was 0.08–0.19 g/km. The strongest impact of an increased amperage level was observed for a combination of low train speed and low contact force.

Considering the consequences on human health, smaller particles are of special concern as they can penetrate deeply into an organism. In this context, the particle mass emissions are usually determined for fractions PM10, PM2.5, and PM1. Therefore, emission factors for these fractions were also derived in the present study. In order to do this, the PM10 mass in the filter samples taken by the PartisolPlus sequential air sampler was determined by weighing the filters before and after the tests. The employed EDM180 particle analyser provided information on the proportions of PM2.5 and PM1 in the PM10 fraction. In order to determine the entire particle mass emission, the recorded particle mass-concentration was related to the return air volume flow, which can be simply calculated as the product of return air velocity (equal to train speed) and the duct cross sectional area (0.08375 m^2). One aspect to be mentioned is the capture of the entire particle emission in the return air duct that could not be guaranteed. However, due to the high return air speed, losses of particles for particles smaller than 10 μm are considered to be low. The derived emission factors of all PM fractions as a function of the applied test configuration are shown in Table 4. As can be seen, the PM10 emission factor is in the range of 0.14 to 0.62 g/km. On average, the respective proportions of PM2.5 and PM1 were found to be 87% and 73%.

4.2. Particle size distribution

4.2.1. Particles smaller than 560 nm

Particle size is an essential parameter in assessing the impact on human health. Ultra-fine particles, in particular, can penetrate deeply into the lungs or even into the bloodstream. However, as such particles do not account for a significant particle mass; they are usually presented in terms of particle number or particle number concentration. Thus, for two selected test cases, particle number concentrations in the range of 5.6 to 560 nm are explained in more detail. The test selection was made with a view to explaining the basic correlations between wear mechanism and particle size distribution.

The particle size distribution was monitored with a 1 Hz resolution, resulting in a certain data pool depending on the test duration. From this, the median value as well as 10th- and 90th-percentile values were calculate. The particle size distribution found in test configuration M (220 km/h|90 N|500A) is shown in Fig. 9. As explained in section 4, emission activity here was dominated by mechanical friction. In addition, this test was performed at the highest speed level, thus resulting in the highest particle number concentration within the group of tests with high contact force and low current intensity. The peak concentration was found to be approx. 16.5 million particles per cubic centimetre (90th percentile value) for a particle size of 10 nm. Starting from this peak, the particle number concentration declines by a factor of ten, both as particle diameter falls to 6 nm, as well as when it increases to 40 nm. A comparison with the particle number concentration during a background measurement showed that the peak concentration also occurred at a particle diameter of approx. 10 nm. However, the peak number concentration in test M was higher by three powers of ten. A comparison of the median value, the 10th percentile and the 90th percentile values shows just a moderate amount of scatter, thus confirming the dominance of mechanical friction in the wear process.

In comparison, Fig. 10 shows the particle size distribution of ultrafine particles for test configuration B (60 km/h|50 N|800A). Due to the low contact force, this test run was subject to the impact of mechanical and electric effects. The high current intensified the effect of the electric arcs and the energy dissipation due to the Joule effect. The increased electric contribution is evident by the presence of a second peak at a particle size of 25–40 nm, where the particle number concentration is similar to that of the first peak. The comparison of the median and percentile values shows a heterogeneous size distribution and significant scattering, caused by recurring electrical events with high particle emissions, and intermediate dominance of mechanical friction with lower emissions. However, due to the significantly lower driving speed compared to test M, the particle number concentration is lower throughout the entire size range.

4.2.2. Particles in the size range 250 nm to 35 μm

Particles of larger fractions than those in the ultrafine range are generally referred to as fine dust. The fractions referred to as fine particles in this section include particles with a diameter of 0.25 to 35 μm. Compared to ultrafine particles, these are present in significantly smaller numbers or are emitted in significantly smaller quantities. However, they are decisive in relation to the emitted mass. Therefore, despite their reduced ability to penetrate deeply into the respiratory tract, these particles are of particular importance.

The particle size distribution was monitored with a 1/6 Hz resolution, resulting in a certain data pool depending on the test duration. From this, the median value as well as 10th- and 90th-percentile values were calculate. Fig. 11 shows the size distribution of the fine particles during test M (220 km/h|90 N|500A). In this test, a well-pronounced peak in the range of 0.3 μm could be observed. Nevertheless, the particle number concentration of roughly 820,000 1/l is significantly lower compared to the peaks in the ultrafine particle range. The comparison of the median and the 90th percentile value again shows good agreement, so that one can again speak of a homogeneous particle size distribution. In comparison, the 10th percentile values are at a significantly lower level (approx. 200,000 1/l). Most of the fine particles are found in the size fraction PM1. The number of particles within the size range of 1 to 10 μm was found to be 2,000 1/l (median).

In contrast, Fig. 12 shows the size distribution of fine particles during test B (60 km/h|50 N|800A). In analogy to the size

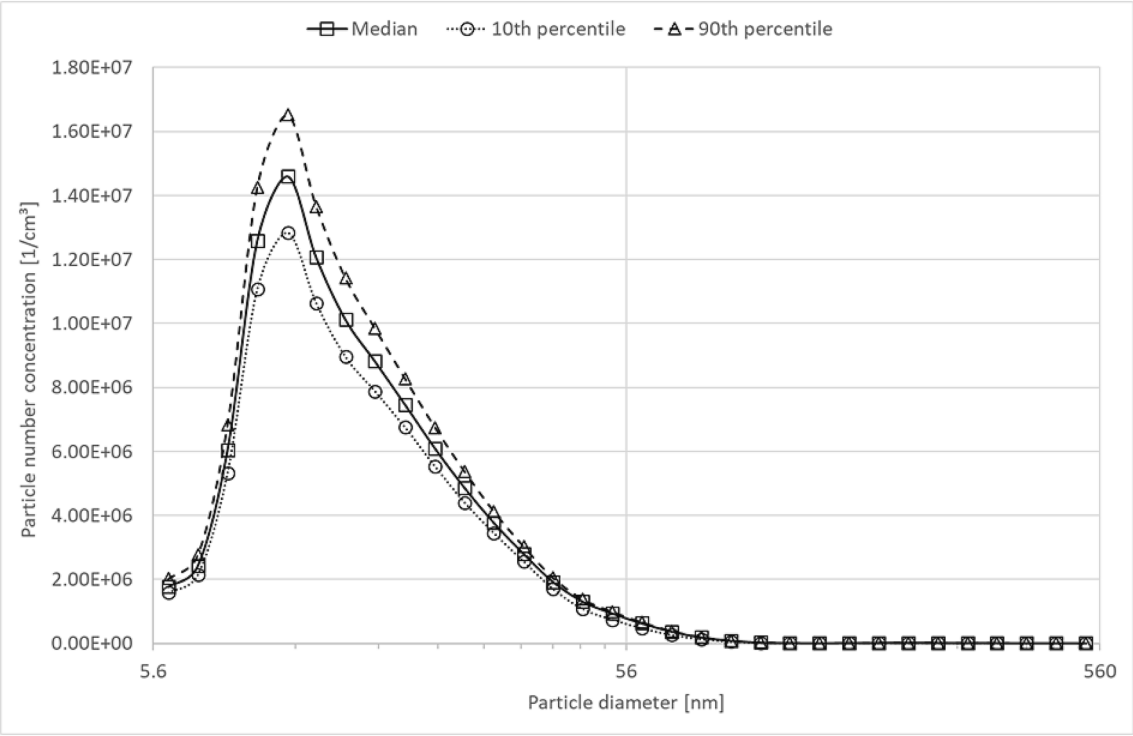

Fig. 9. Particle size distribution of ultrafine particles during a test with test configuration M.

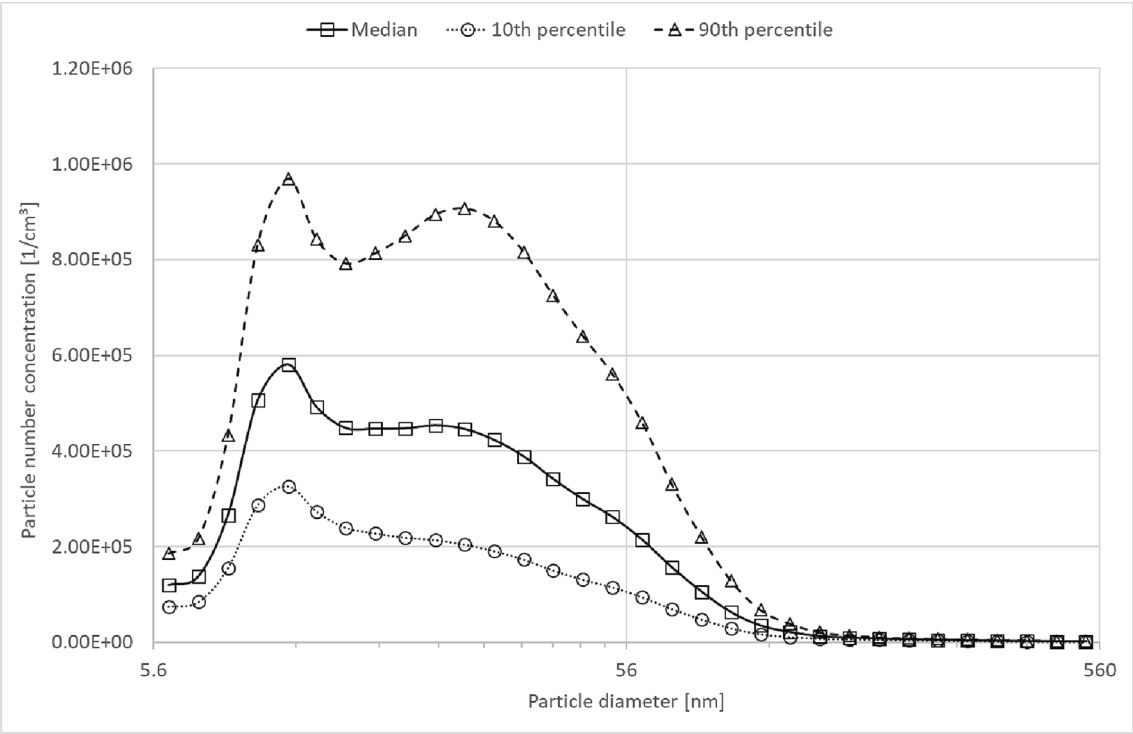

Fig. 10. Particle size distribution of ultrafine particles during a test with test configuration B.

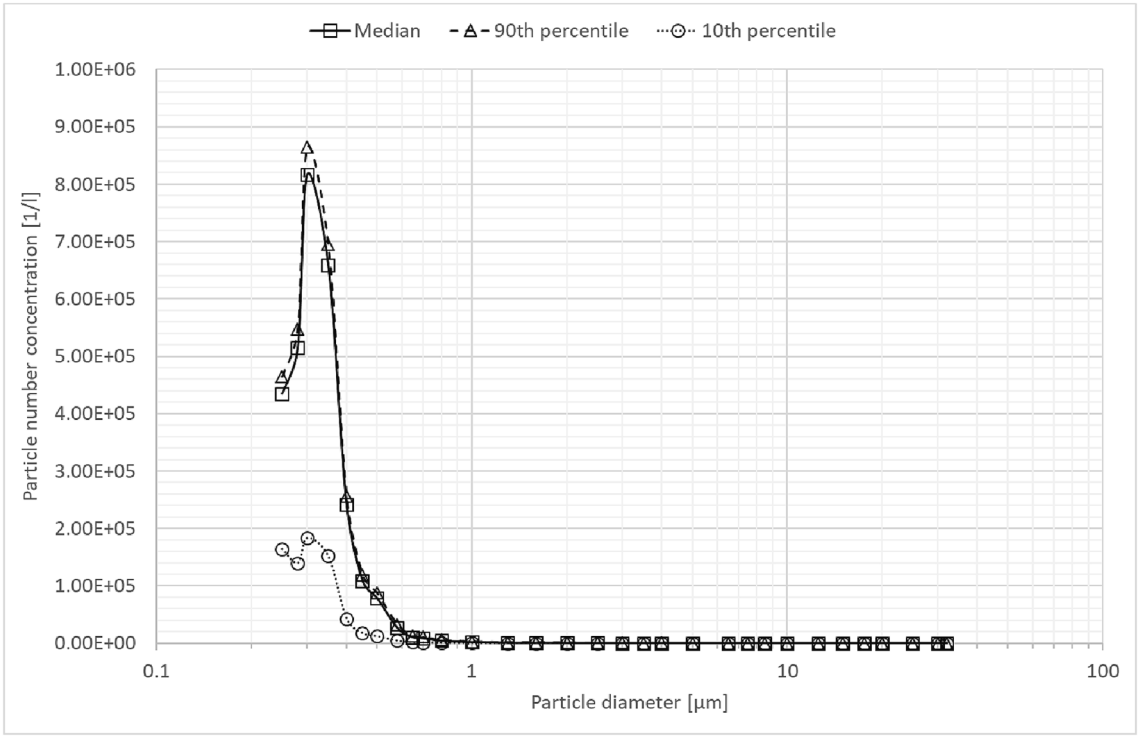

Fig. 11. Particle size distribution of fine particles during a test with test configuration M.

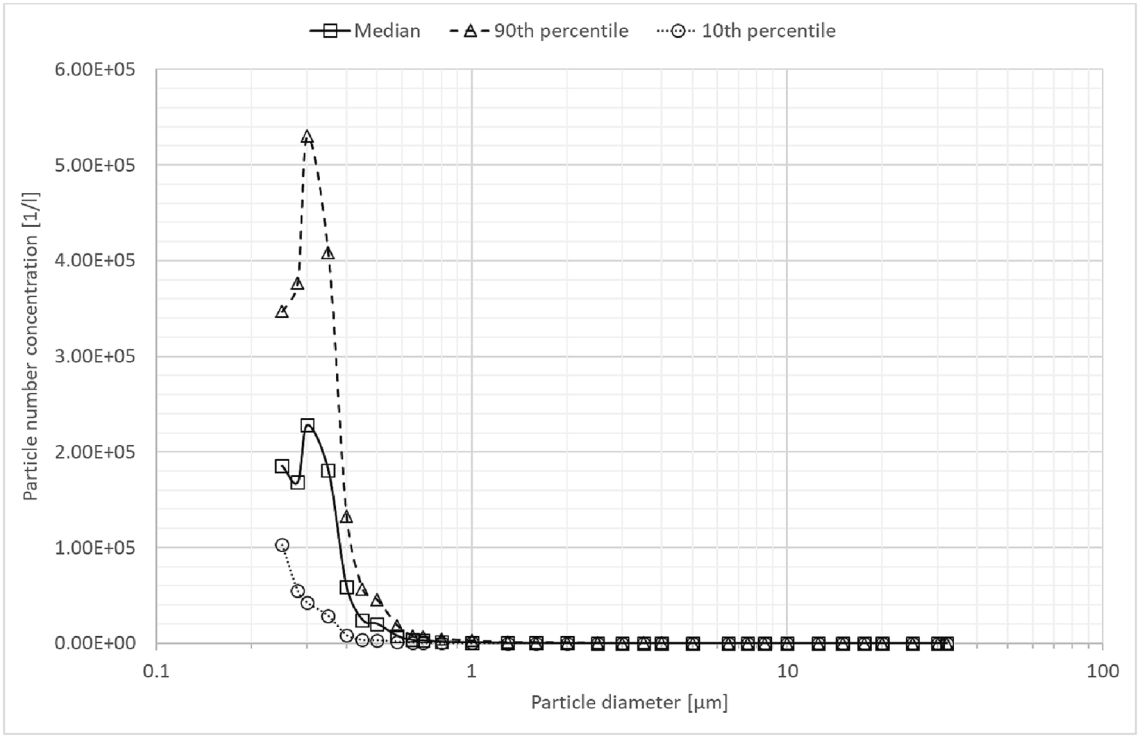

Fig. 12. Particle size distribution of fine particles during a test with test configuration B.

distribution in the ultrafine range (see Fig. 10), the comparison of the median and the percentile values shows large deviations; thus, one can speak of a 'heterogeneous curve'. While the 10th percentile value shows a peak of approx. 223,000 1/l at 0.3 μm, the 90th percentile value in this size range is 525,000 1/l. The number of particles in the size range 1–10 μm was determined to be 886 1/l (median).

4.3. Chemical analysis of particle composition

A chemical analysis of a few selected filter samples provided qualitative information on the contribution of contact wire and contact strip to the total particle emissions. A contact wire made of pure copper (Cu-ETP) and a contact strip made of (20–25%) copper impregnated carbon were used for the CCTB tests. Thus, the chemical analysis was performed for the elements copper (Cu), elemental carbon (EC) and organic carbon (OC). Chemical analysis was carried out for eight selected filter samples. The results from these are presented in Table 5.

On average, a copper content of 40.7% of the total mass was determined. However, a closer look reveals differences depending on the test configuration and on the contribution of the wear mechanisms. While the copper content is relatively constant, in the range of 35.9 to 39.9% for high contact pressure and low contact pressure in combination with low current intensity, the two tests with low contact pressure and high current intensity (Test B and Test F) have to be highlighted owing to their copper content of 47.6 to 51.2%. This indicates that electrical arcs cause particles to be emitted from both the contact strip and the contact wire.

5. Conclusions

A series of tests was conducted using the CCTB at the Politecnico di Milano. These tests enabled unique quantification of particle emissions and improved upon existing estimations based only on mass loss and replacement cycles. The experimental study entailed observation of emitted particle mass, particle size distribution in the range of 5.6 nm to 35 μm, and chemical analysis of particle composition. The information gained was used to derive emission factors for the fractions PM10, PM2.5 and PM1. TSP emission factors were determined on the basis of the mass loss monitored after every test run. Based on the TSP emission factors a parameter study was performed in order to determine the influence of train speed, contact force and current intensity on the particle emissions resulting from wear. The chemical analysis of selected filter samples provided information on the respective emission contributions from contact wire and contact strip to total particle emissions. The main findings from this experimental study are as follows:

- The emissions from the contact between contact wire and contact strip are based on three wear mechanisms. These are mechanical friction, electric arcs and the wear due to the Joule effect.
- The influence of mechanical friction dominates at high contact forces between contact wire and contact strip.
- Emissions due to mechanical friction increase exponentially with increasing train speed.
- Emissions due to electric contributions are favoured by low contact forces and high current intensity.
- Higher contact forces cause lower PM emissions than lower contact forces.
- An increased current intensity increases the emissions due to electric arcs.
- The PM10 emissions range from 0.14 to 0.61 g/km (mean value 0.35 g/km) depending on train speed, contact force and current intensity.
- The shares of the fractions PM2.5 and PM1 in the PM10 emissions are on average 87% and 72.5% respectively.
- The influence of mechanical friction and electric arcs can be determined via the particle diameter characteristics of the wear mechanism.
- Mechanical friction primarily causes particle emissions in the size range of 6–25 nm.
- In comparison, electric arcs cause larger particles (25–90 nm).
- While particles are emitted continuously due to mechanical friction (as evidenced by the similar level of percentile and median values), electric arcs represent individual events (with a large scattering of the particle number concentration).
- The respective mass fractions of the emissions from contact wire and contact strip due to mechanical friction can be roughly stated as 1/4 contact wire and 3/4 contact strip.

Table 5
Results of the chemical analysis for selected filter samples. (OC – organic carbon, EC – elemental carbon, TC – total carbon, Cu – copper).

Test	OC [mass-%]	EC [mass-%]	TC [mass-%]	Cu [mass-%]
A	21.1	41.7	62.8	37.2
B	4.8	44.0	48.8	51.2
E	0.4	62.0	62.4	37.6
F	0.5	51.9	52.4	47.6
G	4.9	57.2	62.1	37.9
H	1.5	58.6	60.2	39.9
K	3.3	60.9	64.1	35.9
L	3.4	57.9	61.3	38.7

- In the case of electric arcs, 37–41% of the emitted particle mass can be attributed to the contact wire, and 59 – 63% to the contact strip. (Note: large difference in the density of copper and carbon).

Finally, it needs to be noted that the influence of wet conditions and ice formation were not investigated. Additionally, a transfer of results to other metal pairings of contact wires and contact strips is only possible to a limited degree.

To provide additional information on the particulate emissions of abrasion in rail transport further investigations at test-benches (wheel-rail, brakes) and field measurements are planned.

Declaration of Competing Interest

The authors declare that they have no known competing financial interests or personal relationships that could have appeared to influence the work reported in this paper.

Acknowledgements:

This study was funded by the German Federal Ministry for Digital Affairs and Transport (BMDV) in the context of the BMDV Network of Experts.

A special thanks to Ms. Anne Kasper-Giebl and her team from the Institute for Chemical Technologies and Analytics at the Vienna University of Technology for chemical analysis of the filter samples.

References

Abbasi, S., Wahlström, J., Olander, L., Larsson, C., Olofsson, U., Sellgren, U., 2011. A study of airborne wear particles generated from organic railway brake pads and brake discs. Wear 273, 93–99. https://doi.org/10.1016/j.wear.2011.04.013.

Abbasi, S., Jansson, A., Olander, L., Olofsson, U., Sellgren, U., 2012a. A pin-on-disc study of the rate of airborne wear particle emissions from railway braking materials. Wear 284–285, 18–29. https://doi.org/10.1016/j.wear.2012.01.016.

Abbasi, S., Olander, L., Larsson, C., Olofsson, U., Jansson, A., Sellgren, U., 2012b. A field test study of airborne wear particles from a running regional train. Proc. Inst. Mech. Eng., F: J. Rail Rapid Transit 226, 95–109. https://doi.org/10.1177/0954409711408774.

Abbasi, S., Jansson, A., Sellgren, U., Olofsson, U., 2013. Particle emissions from rail traffic: a literature review. Crit. Rev. Environ. Sci. Technol. 43, 2511–2544. https://doi.org/10.1080/10643389.2012.685348.

GRIMM Aersol Technik, 2022. EDM 180 partilce analyser,. URL https://www.grimm-aerosol.com/products-en/dust-monitors/approved-pm-monitor/edm180-the-proven/ (accessed 10.22.22).

Allianz pro Schiene e.V., 2022. Elektrifizierung erklärt: Das Schienennetz muss unter Strom stehen. URL https://www.allianz-pro-schiene.de/themen/infrastruktur/elektrifizierung-bahn/ (accessed 10.12.22).

Bucca, G., Collina, A., 2009. A procedure for the wear prediction of collector strip and contact wire in pantograph–catenary system. Wear 266, 46–59. https://doi.org/10.1016/j.wear.2008.05.006.

Bucca, G., Collina, A., 2015. Electromechanical interaction between carbon-based pantograph strip and copper contact wire: A heuristic wear model. Tribol. Int. 92, 47–56. https://doi.org/10.1016/j.triboint.2015.05.019.

Burkhardt, M., Rossi, L., Boller, M., 2008. Diffuse release of environmental hazards by railways. Desalination 226, 106–113. https://doi.org/10.1016/j.desal.2007.02.102.

Cha, Y., Abbasi, S., Olofsson, U., 2018. Indoor and outdoor measurement of airborne particulates on a commuter train running partly in tunnels. Proc. Inst. Mech. Eng., F: J. Rail Rapid Transit 232, 3–13. https://doi.org/10.1177/0954409716642492.

Derosa, S., Navik, P., Collina, A., Bucca, G., Ronnquist, A., 2020. A heuristic wear model for the contact strip and contact wire in pantograph – Catenary interaction for railway operations under 15 kV 16.67 Hz AC systems. Wear 456-457. https://doi.org/10.1016/j.wear.2020.203401.

DZSF, 2022. Größenspezifische und räumliche Verteilung von verkehrsbedingten Abrieben und partikulären Emissionen. URL https://www.dzsf.bund.de/SharedDocs/Standardartikel/DZSF/Projekte/Projekt_44_Abriebe_Emissionen.html (accessed 10.12.22).

Fridell, E., Ferm, M., Ekberg, A., 2010. Emissions of particulate matters from railways – emission factors and condition monitoring. Transp. Res. Part D: Transp. Environ. 15, 240–245. https://doi.org/10.1016/j.trd.2010.02.006.

Fridell, E., Björk, A., Ferm, M., Ekberg, A., 2011. On-board measurements of particulate matter emissions from a passenger train. Proc. Inst. Mech. Eng., F: J. Rail Rapid Transit 225, 99–106. https://doi.org/10.1177/09544097JRRT407.

Fruhwirt, D., Sturm, H., Steiner, H., 2021. Partikelemissionen des Schienenverkehrs – Ergebnisse aus in-situ Messungen in Tunnelanlagen/PM emissions from railway traffic – results of in-situ measurements in tunnels. GrdL 81, 225–233. https://doi.org/10.37544/0949-8036-2021-05-06-71.

Heldestab, J., Kljun, N., 2007. PM10-EMISSIONEN VERKEHR Teil Schienenverkehr (No. 1492A-SYNTHESESBERICHT-070108.DOC). INFRAS AG, Bern.

Heldestab J., 2002. PM10-Emissionen des Verkehrs Statusbericht Teil Schienenverkehr. Bundesamt für Umwelt, Wald und Landschaft, Bern.

Manfred Irsigler, 2014. Qualitätskriterien für Fahrdrähte und Montageprozesse. URL https://www.plassertheurer.com/fileadmin/user_upload/Mediathek/Publikationen/30_39_Irsigler.pdf (accessed 11.14.21).

TSI Incorporated, 2022. Engine Exhaust PArticle SIzer 3090. URL https://tsi.com/products/particle-sizers/fast-particle-sizer-spectrometers/engine-exhaust-particle-sizer-(eeps)-3090/ (accessed 10.22.22).

Wu, Jiqin, 2018. Pantograph and Contact Line System. URL https://www.sciencedirect.com/topics/engineering/carbon-strip#:~:text=Pantograph%20strips%20are%20often%20made,interaction%20with%20the%20contact%20wire.&text=and%20contact%20wire.-,Carbon%20strips%20are%20proved%20to%20be%20the%20most%20suitable%20material,and%20copper%20alloy%20contact%20wires. (accessed 2.17.22).

Knauer, K., Behra, R., Sigg, L., 1997. Effects of free Cu ^{2} + and Zn ^{2} + ions on growth and metal accumulation in freshwater algae. Environ. Toxicol. Chem. 16, 220–229. https://doi.org/10.1002/etc.5620160218.

Kykal, C., Horn, H.G., Tritscher, T., Dahlkötter, F., Farnsworth, J., 2017. Aerosolprobenahme und deren Optimierung. Presentation at Graz University of Technology.

Landesamt für Bergbau, 2012. Tagungsband : 20 Jahre Bodendauerbeobachtung in Niedersachsen 5,24 MB. Energie Geologie. https://doi.org/10.48476/GEOBER_23_2012.

Landesamt für Bergbau, 2021. 30 Jahre Bodendauerbeobachtung in Niedersachsen 18,80 MB. Energie Geologie. https://doi.org/10.48476/GEOBER_39_2021.

Mohsen, M., Ahmed, M.B., Zhou, J.L., 2018. Particulate matter concentrations and heavy metal contamination levels in the railway transport system of Sydney, Australia. Transp. Res. Part D: Transp. Environ. 62, 112–124. https://doi.org/10.1016/j.trd.2018.02.015.

Nirel, P., Pasquini, F., 2021. Differentiation of copper pollution origin: agricultural and urban sources. URL https://hal.archives-ouvertes.fr/hal-03296320 (accessed 12.22.22).

Olofsson, U., Zhu, Y., Abbasi, S., Lewis, R., Lewis, S., 2013. Tribology of the wheel–rail contact – aspects of wear, particle emission and adhesion. Veh. Syst. Dyn. 51, 1091–1120. https://doi.org/10.1080/00423114.2013.800215.

Politecnico di Milano, 2023. The Current Collection Test Bench (CCTB) of PoliMi. URL https://www.mecc.polimi.it/en/about-us/news/the-current-collection-test-bench-cctb-of-polimi (accessed 1.3.23).

Richter, F., Schmidt, W., Wolf, P., 2012. Emissionen des Schienenverkehrs in Sachsen Schriftenreihe, Heft 2/2012. Sächsisches Landesamt für Umwelt, Landwirtschaft und Geologie (LfULG), Dresden.

Samarska, A., Kovrov, O., Zelenko, Y., 2020. Investigation of heavy metal sources on railways: ballast layer and herbicides. J. Ecol. Eng. 21, 32–46. https://doi.org/10.12911/22998993/127393.

Siemens Mobility Global, 2021. Produktkatalog - Fahrleitungsmaterial für den Nah- und Fernverkehr. URL https://assets.new.siemens.com/siemens/assets/api/uuid:733a4bf7-36f8-4357-ba84-895897260f65/siemens-fahrleitungsmaterial-kat-de.pdf (accessed 2.17.22).

Söderberg, A., Wahlström, J., Olander, L., Jansson, A., Olofson, U., 2008. On Airborne Wear Particles Emissions of Commercial Disc Brake Materials – A Pin on Disc Simulation (No. ISSN 1400–1179). Department of Machine Design Royal Institute of Technology, Stockholm.

Sturm, P., Fruhwirt, D., Steiner, H., 2022. Impact of dust loads in long railway tunnels: In-situ measurements and consequences for tunnel facilities and operation. Tunn. Undergr. Space Technol. 122, 104328 https://doi.org/10.1016/j.tust.2021.104328.

Thermo Fisher Scientific Inc, 2021. PartisolPlus 2025i - Sequential Air Sampler. URL https://corporate.thermofisher.com/content/tfcorpsite/us/en/index/about.html (ac-cessed 10.22.22).

Zingelmann M., Karthe M., Pedrosa L., Scheytt T., Hitzschold S., 2022. Einstufung von Niederschlagswasser auf Streckengleisen - Quantifizierung und Charakterisierung der Abflussmenge und chemischen Zusammensetzung von Niederschlagswasser. 10.48755/dzsf.220019.01.